Journal of Biomedical Optics

SPIEDigitalLibrary.org/jbo

Multifunctionality of indocyanine green-loaded biodegradable nanoparticles for enhanced optical imaging and hyperthermia intervention of cancer

Ronak H. Patel
Aniket S. Wadajkar
Nimit L. Patel
Venkaiah C. Kavuri
Kytai T. Nguyen
Hanli Liu

SPIE

Multifunctionality of indocyanine green-loaded biodegradable nanoparticles for enhanced optical imaging and hyperthermia intervention of cancer

Ronak H. Patel,* Aniket S. Wadajkar,* Nimit L. Patel, Venkaiah C. Kavuri, Kytai T. Nguyen, and Hanli Liu
University of Texas, Department of Bioengineering, Joint Graduate Program between University of Texas at Arlington and University of Texas Southwestern Medical Center at Dallas, Texas 76019

Abstract. The aim of this study was to develop and characterize multifunctional biodegradable and biocompatible poly lactic-co-glycolic acid (PLGA) nanoparticles loaded with indocyanine green (ICG) as an optical-imaging contrast agent for cancer imaging and as a photothermal therapy agent for cancer treatment. PLGA-ICG nanoparticles (PIN) were synthesized with a particle diameter of 246 ± 11 nm, a polydispersity index of 0.10 ± 0.03, and ICG loading efficiency of $48.75 \pm 5.48\%$. PIN were optically characterized with peak excitation and emission at 765 and 810 ± 5 nm, a fluorescence lifetime of 0.30 ± 0.01 ns, and peak absorbance at 780 nm. The cytocompatibility study of PIN showed 85% cell viability till 1-mg/ml concentration of PIN. Successful cellular uptake of ligand conjugated PIN by prostate cancer cells (PC3) was also obtained. Both phantom-based and *in vitro* cell culture results demonstrated that PIN (1) have the great potential to induce local hyperthermia (i.e., temperature increase of 8 to 10°C) in tissue within 5 mm both in radius and in depth; (2) result in improved optical stability, excellent biocompatibility with healthy cells, and a great targeting capability; (3) have the ability to serve as an image contrast agent for deep-tissue imaging in diffuse optical tomography. [DOI: 10.1117/1.JBO.17.4.046003]

Keywords: indocyanine green; biodegradable nanoparticles; optical imaging contrast; hyperthermia; diffuse optical imaging.

Paper 11441 received Aug. 15, 2011; revised manuscript received Jan. 30, 2012; accepted for publication Feb. 13, 2012; published online Apr. 9, 2012.

1 Introduction

Ability to detect cancer at an early stage saves many lives and motivates the development of exogenous optical contrast agents that are specific to cancer. The availability of such fluorophores in near infrared (NIR) region (700 to 900 nm) offers several advantages for optical imaging, which can be a possible candidate for minimally invasive diagnosis of cancer with avoidance of harmful radiation at relatively low cost.[1] In addition, the capability of NIR light to penetrate several centimeters in biological tissue provides an excellent noninvasive imaging modality for cancer detection with good sensitivity and reasonable resolution. Finding, characterizing, and validating specific probes that can emit light in the NIR range would enhance imaging sensitivity at significant depths of tissue.[2,3] This motivates us toward development of multifunctional poly lactic-co-glycolic acid (PLGA) nanoparticles encapsulating indocyanine green (ICG), which can serve as a NIR exogenous contrast and thermal agent specific for cancer diagnosis and treatment.

ICG is an amphiphilic tricarbocyanine NIR dye. It is a widely investigated contrast agent and is approved by U.S. Food and Drug Administration (FDA) for diagnostic imaging in humans.[4,5] Being a fluorescence dye, when being irradiated, ICG strongly absorbs light at 780 nm and emits light at 820 nm.[2,3] Recently, much focus is paid on the fluorescence property of ICG that serves as a contrast agent for tumor imaging. Moreover, the strong absorption of NIR light makes it suitable for diffuse optical tomography (DOT)[6] and photoacoustic (PA) imaging.[7] Apart from special optical properties, it has shown excellent thermal properties. When being irradiated by light, ICG absorbs light and converts it into heat, which can be used for photothermal treatments.[3] Hence, photodynamic therapy using ICG serves as a promising method for the destruction of tumors.[3,4,8] However, ICG is prone to aqueous instability and photo-bleaching, has a low quantum yield, and is not target specific, all of which limit its applicability for prolonged target specific applications.[5,7]

In recent years, biodegradable-biocompatible, FDA-approved PLGA carriers are one of the most common particulate systems employed to enhance ICG for quantitative imaging and therapeutic applications.[5,7,9] PLGA nanoparticles are associated with enhanced permeation and retention (EPR) effect that allows passive targeting from the blood stream into the tumor site.[5,10,11] In addition, targeting ligands can be conjugated to PLGA nanoparticles to make them cancer specific.[5,7,9] ICG encapsulation by PLGA nanoparticles effectively protects ICG from aggregation and protein interaction, thereby stabilizing the optical characteristics of ICG. It not only preserves the aqueous, thermal, and photo-stability of ICG but also increases the circulation half-life to ~14 min, which is three to seven times more than that of free ICG.[5]

The presented work is mainly focused on the characterization of a multifunctional nanoparticulate system entrapping ICG within the PLGA reservoir, followed by exploration on its cancer targeting ability for tumor imaging and therapeutic ability for

Address all correspondence to: Hanli Liu, Department of Bioengineering, Joint Graduate Program between University of Texas at Arlington and University of Texas Southwestern Medical Center, Texas 76019, USA. Tel: (817) 272-2054; Fax: 817 272 2251; E-mail: hanli@uta.edu.
*These authors contributed equally.

0091-3286/2012/$25.00 © 2012 SPIE

hyperthermia treatment based on the absorption characteristics. Specifically, we report (1) fabrication process and characterization of PLGA-ICG nanoparticles (PIN); (2) its optical characterization of excitation-emission matrix, fluorescence lifetime, and aqueous stability; (3) biocompatibility and cellular uptake of PIN after ligand binding; (4) the unique application of PIN as an imaging contrast to enhance DOT based on their high-absorption capability in the NIR range; (5) the feasibility of PIN as a thermal ablation agent for cancer treatment using laboratory phantoms.

2 Materials and Methods

Poly lactic-co-glycolic acid (DLG-4A, L:G 50:50; i.e., 50% lactic acid +50% glycolic acid) was purchased from Lakeshore Biomaterials, AL, USA. The molecular weight is related to the inherent viscosity. In our case, the inherent viscosity of PLGA was 0.35 to 0.45 dL/g. Indocyanine green, polyvinyl alcohol (PVA, 87% to 89% anhydrous), dichloromethane (DCM, 99.8% anhydrous), N-hydroxysulfosuccinimide (NHS), 1-[3-(Dimethylamino)-propyl]-3-ethyl carbodiimide hydrochloride (EDC), and Dulbecco's modified eagle medium (DMEM) supplemented with 10% serum and 1% penicillin–streptomycin were of reagent grade and purchased from Sigma-Aldrich (St. Louis, MO).

2.1 *Synthesis of PIN*

For nanoparticle synthesis, double-emulsion technique, as shown in Fig. 1(a), was used to entrap aqueous ICG solution within PLGA reservoir.[7,9] The first emulsion (water-in-oil) was prepared by adding aqueous ICG solution (1.03-mM ICG in 1-ml de-ionized water) drop-wise to the organic phase of PLGA (90-mg PLGA in 3-ml DCM) under vigorous and continuous stirring, followed by homogenization by a sonicator (BioLogics Inc., Manassas, VA) at 30 W for 3 min. This first emulsion was then added drop-wise to aqueous PVA solution (5% w/v PVA in 12-ml de-ionized water) to form the second emulsion (water-in-oil-in-water). After an hour of stirring at room temperature, the formed particles were washed twice using ultracentrifuge (25,000 rpm for 20 min) to get rid of free ICG. After nonencapsulated ICG present in the supernatant was removed, the synthesized PIN were stored at −20 °C for later analysis. In order to separate nanoparticles from aggregates, additional centrifugation was performed (4000 rpm for 5 min); supernatant containing nanoparticles were collected. The nanoparticles were then lyophilized using a FreeZoneBenchtop Freeze Dry Systems (Labconco Corp., Kansas City, MO) to obtain the powder form of PIN.

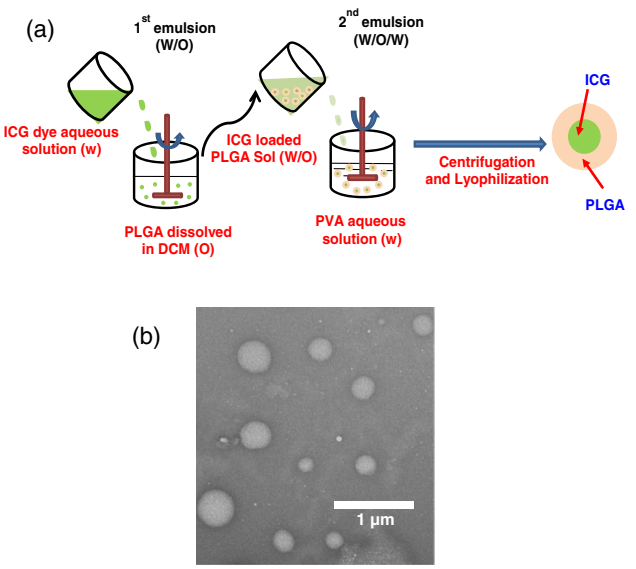

Fig. 1 (a) Demonstration of a double-emulsion process for the synthesis of PIN. ICG aqueous solution (in Water: W) is added in PLGA organic phase solution (in Oil: O) that forms the first emulsion (i.e., Water in Oil: W/O). The first emulsified solution is added in PVA aqueous solution to form the second emulsion (i.e., Water in Oil in Water: $W/O/W$), which is further processed to form ICG loaded PLGA nanoparticles; (b) TEM image presenting the morphology of PIN.

2.2 *Conjugation of PIN with Targeting Ligands*

The formed nanoparticles were conjugated with different targeting ligands to determine the uptake efficiency by PC3 cells (prostate cancer cells). PIN were conjugated with (1) RGD-4C peptides that are specific to $\alpha_5\beta_3^+$ cells[12]; (2) folic acid that targets the folate receptors on surfaces of tumor cells;[12] and (3) R11 peptides that are cell-penetrating peptides specific to prostate cancer cells.[13] For conjugation, 10-mg PIN were suspended in 1 ml of PBS followed by addition of 200-mM (40 mg) NHS and 400-mM (80 mg) EDC. After one hour of incubation on an orbital shaker at room temperature, 1 μM of RGD-4C, R11 or folic acid were added, and the reaction was continued for 12 h at room temperature. The ligand-conjugated PIN were washed and collected as previously described.[14,15]

2.3 *Characterization of PIN*

The formed PIN were characterized for their structural morphologies. The particle size, polydispersity index, and zeta potential were obtained using ZetaPALS photon correlation spectroscopy (Brookhaven Instruments Corporation, Holtsville, NY). The structural morphology of PIN was further verified using a transmission electron microscope (TEM, FEI Tecnai G^2 Spirit BioTWIN, Hillsboro, OR). PIN were diluted thoroughly in distilled (DI) water to make a final concentration of 1 mg/ml, and the sample was analyzed in terms of its size and shape.

The ICG loading efficiency was evaluated to determine the amount of ICG dye encapsulated in PIN indirectly. ICG standards (0.5 to 10 μg/ml of ICG solution) were prepared by dispersing ICG in DI water. A spectrophotometer (Infinite M200, TECAN, Switzerland) was used to measure the fluorescence intensity of the ICG standard solutions and supernatant after PIN formation. Fluorescent intensity of the solutions was measured at an excitation of 780 nm and emission at 810 nm. A calibration curve was established between different ICG concentration and their fluorescence intensity. The calibration curve was thus used to measure the ICG amount present in the supernatant. Loading efficiency of PIN was quantified by an indirect method by measuring the amount of ICG present in the supernatant, as shown in Eq. (1).

$$\text{ICG Loading efficiency}(\%) = \frac{\text{Amount of ICG used} - \text{Amount of ICG in supernatant}}{\text{Amount of ICG used}} \times 100. \quad (1)$$

2.4 *Optical Characterization of PIN*

In order to study the behavior of ICG and PIN in different solvents, excitation and emission spectrum of ICG and PIN dissolved in biorelevant solvents were determined using spectrofluorophotometer RF-5301PC (Shimadzu Scientific Instruments, Columbia, MD). ICG (20 μg/ml) and PIN (1 mg/ml) were dissolved in cell medium, phosphate buffer saline (PBS), and DI water; their excitation and emission spectra were obtained at emission of 810 nm and excitation at 780-nm wavelength, respectively. Further, the difference of material degradation over time between PIN and ICG was investigated using spectrophotometer. ICG (50 μg/ml) and PIN (1.5 mg/ml) were dissolved in DI water, PBS, and saline. Fluorescence measurements were taken over a period of time using the spectrophotometer. The effect of solvents on fluorescence emission for ICG and PIN were compared at different time points. To reduce the degradation, we often stored PLGA nanoparticles as powder form in the freezer −20 °C. If it was in solution, then we stored them at −4 °C, but only for a short period of time. For degradation study, we incubated nanoparticles with water or buffer at 37°C, which is similar to the body temperature in order to perform the study under real physiological conditions. If PLGA nanoparticles contained dyes during the sample preparation, they were protected from light by being covered and stored in a dark place. Moreover, the absorption spectra of ICG and PIN were determined using a spectrophotometer (Lambda 20, PerkinElmer Inc., CT). ICG (37.5 μg/ml) and PIN (3.45 mg/ml) were dissolved in water, and the absorption spectra were measured between 400 to 900 nm. The decrease in absorbance of ICG and PIN was measured over a period of time. The maximum absorbance obtained from the absorbance spectra were compared between ICG and PIN.

Fluorescence lifetime is an important parameter to know while imaging two fluorophores with similar emission wavelengths.[16] Hence we investigated the lifetime of ICG and PIN to understand the dependence of lifetime on fluorophore concentration and also the effect of PLGA on the lifetime of ICG dye. Initially, ICG (25, 50, and 75 μg/ml) and PIN (5, 7.5, and 10 mg/ml) were dissolved in water for lifetime measurements. A time-gated, ultrafast Intensified CCD (ICCD) camera was employed to measure fluorescence lifetime. The experimental setup is shown in Fig. 2(a). Samples were excited with a 50 picosecond (ps) broadband-pulsed laser (SC-450, Fianium Inc., Eugene, OR) filtered by a 780 ± 10 nm excitation filter. Emitted light was filtered by an 820 ± 10 nm emission filter. Images were captured at every 0.05 ns for a period of 5 ns by the ICCD camera. In addition, the system-response function was also captured by irradiating a white sample with the laser and acquiring the reflectance from the white sample. The system-response function was used to de-convolve with the acquired data from ICG and PIN and to give rise to the resulting time-dependent fluorescence of ICG and PIN, respectively. Then these time-dependent fluorescence profiles were fitted to a single-exponential model so as to obtain fluorescence lifetime using the following equation:[16]

$$\text{Intensity}(I) = \alpha e^{\left(-\frac{t}{\tau}\right)}, \tag{2}$$

where τ is the fluorescence lifetime, α is the fluorescence intensity, and t is the time at which images were acquired.

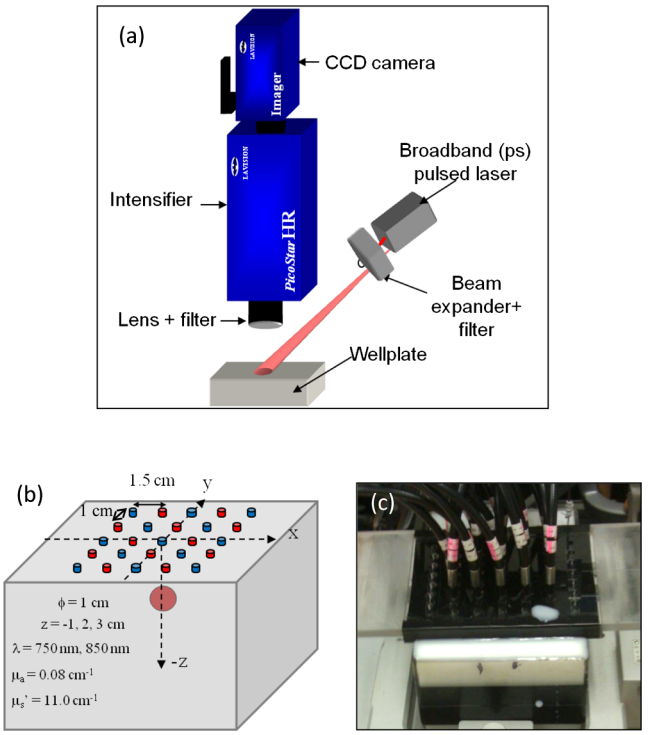

Fig. 2 (a) Schematic of the experimental setup for fluorescent lifetime measurements of ICG and PIN; (b) schematic of the experimental setup for the DOT phantom study: blue markers (= 13) are for sources and red markers (= 12) are for detectors. The source-detector optode separations are 1.5 and 1 cm along x axis and y axis, respectively; (c) a photo showing the actual setup for the DOT phantom study. The diameter of PIN-containing sphere was 0.9 cm.

2.5 *In Vitro Studies*

Cytocompatibility study was performed to evaluate the toxicity of PIN. Human dermal fibroblasts (HDFs) were cultured in DMEM supplemented with 10% serum and 1% penicillin-streptomycin and maintained at 37°C, 5% CO_2 in the humid atmosphere of an incubator. Nanoparticle suspensions made in various known concentrations (0, 0.1, 0.25, 0.3, 0.5, 1, 2.5, and 5 mg/ml) were added to the cells. The cells were further incubated at 37°C, 5% CO_2 for six hours and 24 h, respectively. At the end of the incubation time, the nanoparticle suspensions were removed, and the cell viability was determined using MTS assays (CellTiter 96® AQ_{ueous} One Solution Cell Proliferation Assay, Promega, WI). Cells exposed to complete media without any nanoparticles served as control samples.

Thereafter, the cellular uptake of PIN by prostate cancer cells was investigated. PC3 cells [American Type Culture Collection (ATCC)] were seeded on sterilized glass slides and incubated at 37°C and 5% CO_2 for 24 h. Cell medium was then changed with media containing PIN, and the cells were further incubated for four hours. Thereafter, cell medium was removed, and the glass slides were washed twice with PBS thoroughly to make sure that nanoparticles from the surface were removed. Fluorescence lifetime imaging microscopy (FLIM) (LSM 710, Carl Zeiss Microimaging LLC., Thornwood, NY) was performed at 705 nm for excitation and 780 nm for emission.

In addition, a cellular uptake of PIN conjugated with three different ligands was examined to understand the targeting ability of PIN. PC3 cells were cultured in RPMI media and

were allowed to grow till confluency. The conjugated and nonconjugated PIN solutions (50, 100, 200, 300, 500, and 1000 μg/ml) prepared in RPMI media were added to the cells and incubated. After two hours of incubation, the media was removed, and the cells were washed thrice with PBS. 300 μl of triton was added in each well to kill the cells. 100 μl from the cell lysis solution was analyzed by a spectrophotometer to obtain the fluorescence intensity measurements of ICG present within the PIN that were uptaken by the cells. Another 100 μl cell lysis solution was further analyzed for the total DNA content by a Pico green DNA assay (Invitrogen Corporation, CA). The ICG characterization curve was used to calculate the amount of ICG present in the nanoparticles. The cellular uptake results were computed from the fluorescence intensity of ICG present in nanoparticles and normalized with the DNA content per sample.

2.6 *Phantom Studies*

2.6.1 *Preparation of tissue phantoms*

We next explored the feasibility of PIN to serve as a DOT contrast agent and thermal ablation agent by performing laboratory experiments. In the beginning, two kinds of solutions were prepared: (1) ICG (0.1, 0.3, and 0.5 mg) in 2-ml intralipid (20%), and (2) PIN (25, 40, and 55 mg) in 2-ml intralipid (20%). 25-mg paraformaldehyde was added to each of these solutions to achieve a higher melting point for phantoms during laser irradiation. In order to prepare the tissue-mimicking phantom, 2 g of gelatin powder was added into 10 ml of boiling water. Once gelatin was completely dissolved in water, it was cool down to 45°C. Finally, the prepared mixtures of 2-ml intralipid containing either ICG or PIN were homogenously mixed with the gelatin solution. This grand mixture was transferred in a glass beaker (2.5 cm in diameter, 3.0 cm in height) to form a cylindrical gelatin phantom or mold. The molds were refrigerated at 4°C for about an hour. In addition, a control phantom was made without PIN/ICG using the same synthesis process for comparisons. The prepared control, PIN (2.08, 3.33, and 4.58 mg/ml), and ICG (0.008, 0.025, 0.041 mg/ml) phantoms were further used for thermal ablation experiments. A spherical mold with a diameter of 0.9 cm containing PIN (2.08 mg/ml) was made to create an absorbing sphere for DOT imaging experiment.

2.6.2 *Quantification of PIN as DOT contrast agent*

Ability to enhance image contrast by PIN for DOT was investigated using a rectangular tank of $10 \times 20 \times 15$(width$\times$ length $\times$ height) cm^3. It was filled with 1% intralipid, having absorption and reduced scattering coefficients of 0.03 cm^{-1} and 10 cm^{-1}, respectively.[6] An array of 13 sources and 12 detectors were arranged in a 5-x-5 matrix with the column-wise separation of 1.5 cm and row-wise separation of 1 cm on the phantom surface [Fig. 2(b) and 2(c)]. In the beginning, the prepared 0.9-cm-diameter gelatin sphere was placed at the bottom of the tank (~14 cm below the probe array); optical baselines were taken for 30 sec at 750 and 850 nm using a DOT imager (Cephalogics LLC, Boston, MA). The sphere was then introduced to 3-cm depth from the tank surface and data captured for 30 sec. The same procedure was repeated two times with the sphere at 2- and 1-cm depths. Changes in optical density (ΔOD) at all sphere depths with respect to the baselines were quantified and used to reconstruct two-dimensional (2-D) DOT images by MATLAB-based graphical user interface (HomER).[17] The final reconstructed images were obtained at the cutoff threshold of 80% of maximum.

2.6.3 *Quantification of PIN as photo thermal agent*

Hyperthermia has been studied as a choice for cancer treatments with various heating sources, such as microwaves, focused ultrasound waves, radio waves, and NIR lasers.[10,11,18] Here we report the feasibility of using PIN as a thermal therapy agent to greatly induce local heating. We inserted thermocouple wires (Omega Technologies Inc., Stamford, CT) 3, 5, and 7 mm, respectively, below the top surface of the phantom for depth measurements as well as 3, 5, and 7 mm laterally away from the laser tip for distance measurements, as shown in Fig. 3(a) to 3(c). The temperature was continuously recorded using a data logger (Hydra Fluke). A continuous-wave laser at 808 nm (Coherent Inc., Santa Clara, CA) was used, irradiating the phantom about an area of 2.26 mm^2 on the top surface of phantoms. The irradiated area was calculated from the numerical aperture of the fiber (0.22), diameter of the fiber (800 μm), and the distance between the laser fiber and phantom (2 mm). The laser power was set at 0.8 W, and the phantom was continuously irradiated for 5 min. The transient temperature changes were monitored at every 5 sec during the entire irradiation period (i.e., 5 min) for control ICG as well as PIN phantoms with different concentrations in order to monitor the thermal changes of ICG and PIN samples with respect to the control sample.

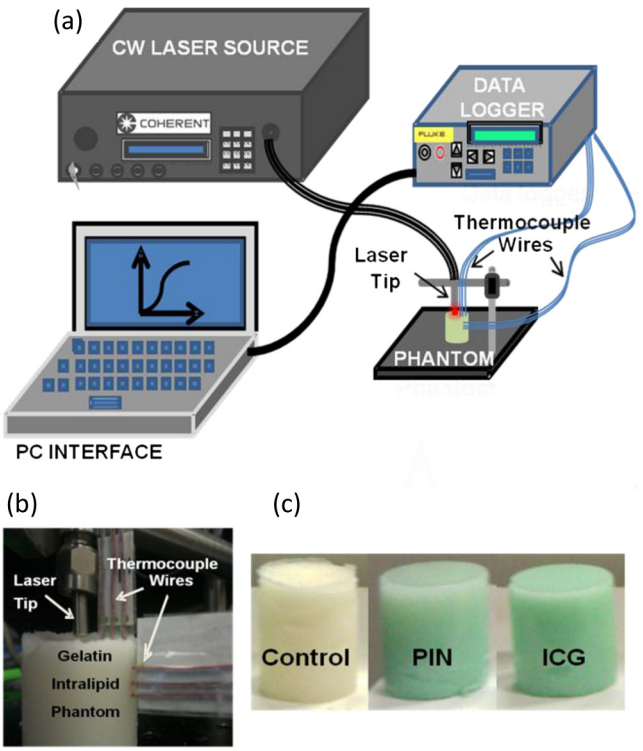

Fig. 3 (a) Schematic of the experimental setup and (b) actual setup for the thermal ablation study using (c) control, PIN, and ICG tissue phantoms.

3 Results and Discussion

3.1 *Nanoparticle Characterization*

The nanoparticles were formed with a mean particle size of 246 ± 11 nm ($n = 3$) and with a polydispersity index of 0.10 ± 0.03 ($n = 3$), showing minimal variation in particle size. The surface charge of PIN was found to be -18 mV, which infers the good stability and midrange polydispersity of PIN. The TEM image of PIN, as shown in Fig. 1(b), confirms the spherical shape and smooth surface of PIN. Moreover, the uniform particle size observed from TEM was in 250- to 300-nm range, which was in close proximity with the particle size obtained from DLS measurement. Further, the ICG loading efficiency as calculated from Eq. (1) was found to be $48.8 \pm 5.5\%$. It confirms that half of ICG used was entrapped in the nanoparticles. The loading efficiency of ICG depends on the amount of PLGA used; hence, a higher loading efficiency can be obtained by increasing the amount of PLGA during fabrication of PIN.[4] Our loading efficiency obtained was higher than that reported by Saxena et al. (9.92%) who had used a direct method.[19]

3.2 *Optical Characterization of PIN*

The excitation-emission spectra of ICG and PIN in different solvents were obtained and compared. As observed in Fig. 4(a) for ICG, excitation spectra were similar and consistent for all the solvents with a peak excitation at 765 nm. Whereas, the emission spectra were shifted toward the longer wavelength, with an emission peak of 805 nm for media, 810 nm for PBS, and 815 nm for water. These results are in good agreement with the previously published data by Altinoglu et al.,[2] who reported that the shift in spectra induced by different solvents was due to specific solvent effects, such as molecule–molecule interactions and hydrogen bonding. As observed from Fig. 4(b), similar spectral characteristics were obtained from PIN spectra (dissolved in media, PBS, and water) with respect to those seen from ICG spectra. This observation implies that no significant effect of PLGA is on the excitation-emission properties of ICG.

Aqueous stability in terms of fluorescence emission was investigated for ICG and PIN in different solvents. Fig. 4(c) and 4(d) show the fluorescence emission of ICG and PIN over a period of time. These figures clearly reveal that a significant

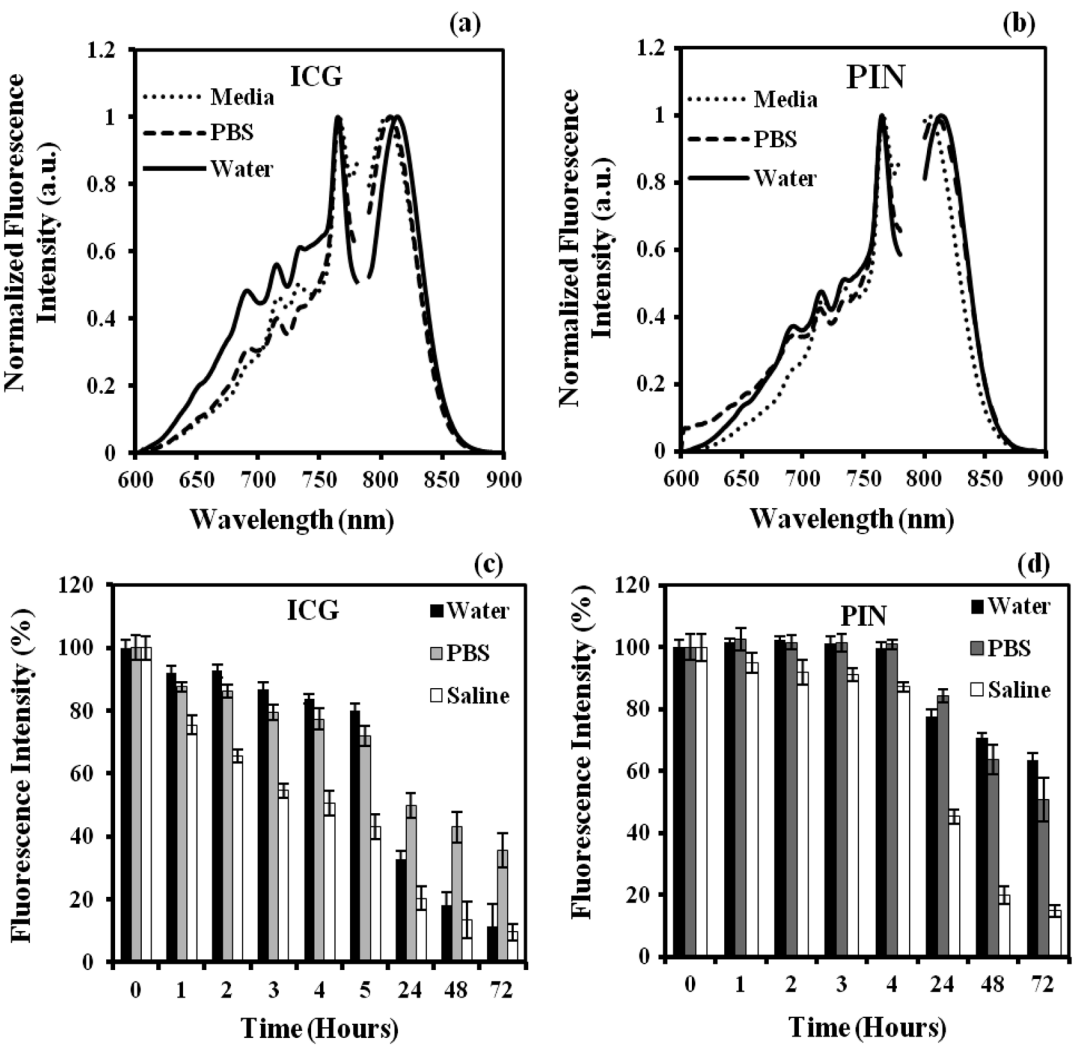

Fig. 4 Averaged excitation and emission spectra of (a) ICG and (b) PIN dissolved in bio-relevant solvents such as media, water, and PBS ($n = 3$). Averaged fluorescence intensity decays of (c) ICG and (d) PIN with respect to time in three different solvents, water, PBS, and saline ($n = 4$). The error bars are obtained by standard errors of mean.

decrease in fluorescence intensity occurs after day one in both cases, but the intensity was dropping off much slower in PIN than the ICG. Also, we observed that the fluorescence intensity of ICG and PIN in saline reduced relatively faster, whereas better stability was achieved in PBS and water. Hence the type of solvent affected the stability of ICG, which could be due to the molecule bonding with the solvent. Overall, ICG dissolved in all three solvents show less aqueous stability as compared with PIN. These results support the fact that PLGA improves the stability of ICG in PIN in aqueous conditions and also preserves the fluorescence property of ICG.[2,3]

Figure 5(a) and 5(b) show the absorption spectra changes of ICG and PIN during a time period of five days. The changes observed in absorption spectra of ICG with respect to time are attributed to self aggregation between ICG monomers and dimers. These changes were not found in PIN since ICG monomers are bound to PLGA, so no self-aggregation occurred.[3] We also observed that the absorbance of ICG decreases faster as compared with PIN. The maximum absorbance of both ICG and PIN was obtained at 780 nm between 700 nm and 850 nm, as seen from Fig. 5(a) and 5(b). In addition, it was observed that concentration of PIN was 100-fold more than ICG, while the maximum absorbance of PIN was less than ICG. This can be explained by the amount of ICG encapsulated in PIN. According to the loading efficiency of ICG, the amount of ICG present in 1.15 mg of PIN (with absorbance $= 0.74 \pm 0.02$) was 6.57 μg, which was less than the used 12.5 μg of ICG (with absorbance $= 1.3 \pm 0.05$). Also, PLGA coating on ICG in PIN may reduce the absorbance of PIN. Moreover, Fig. 5(c) and 5(d) show the maximum absorbance at 780-nm wavelength with different concentrations of ICG and PIN, respectively. In each figure, the slope of absorbance decay was calculated by fitting a linear regression for each concentration of ICG and PIN. Since the decrease in absorbance with time (i.e., slope) followed a similar pattern for all concentrations of ICG as well as PIN, the mean of the slopes was calculated for three concentrations of ICG and PIN, respectively. The mean slope for ICG was 0.33 ± 0.1 (1/day) whereas for PIN it was 0.10 ± 0.02 (1/day), showing the absorbance of ICG decays with time three times faster than that of PIN. Thus these results signify that PLGA not only preserves absorption property of ICG in PIN but also reduces the decay rate of ICG within PIN.[2,3]

The fluorescence lifetime of ICG and PIN were measured at different concentrations. Figure 6(a) shows normalized fluorescence decay curves for three different concentrations of ICG and PIN. It is visually observed that there was no change in the decay curve with the change in fluorophore concentration for each of the two cases. It is also observed that PIN takes a little longer time to decay than ICG when returning back to the ground state. Figure 6(b) displays quantitative lifetime values, calculated using Eq. (2), of ICG and PIN at the three

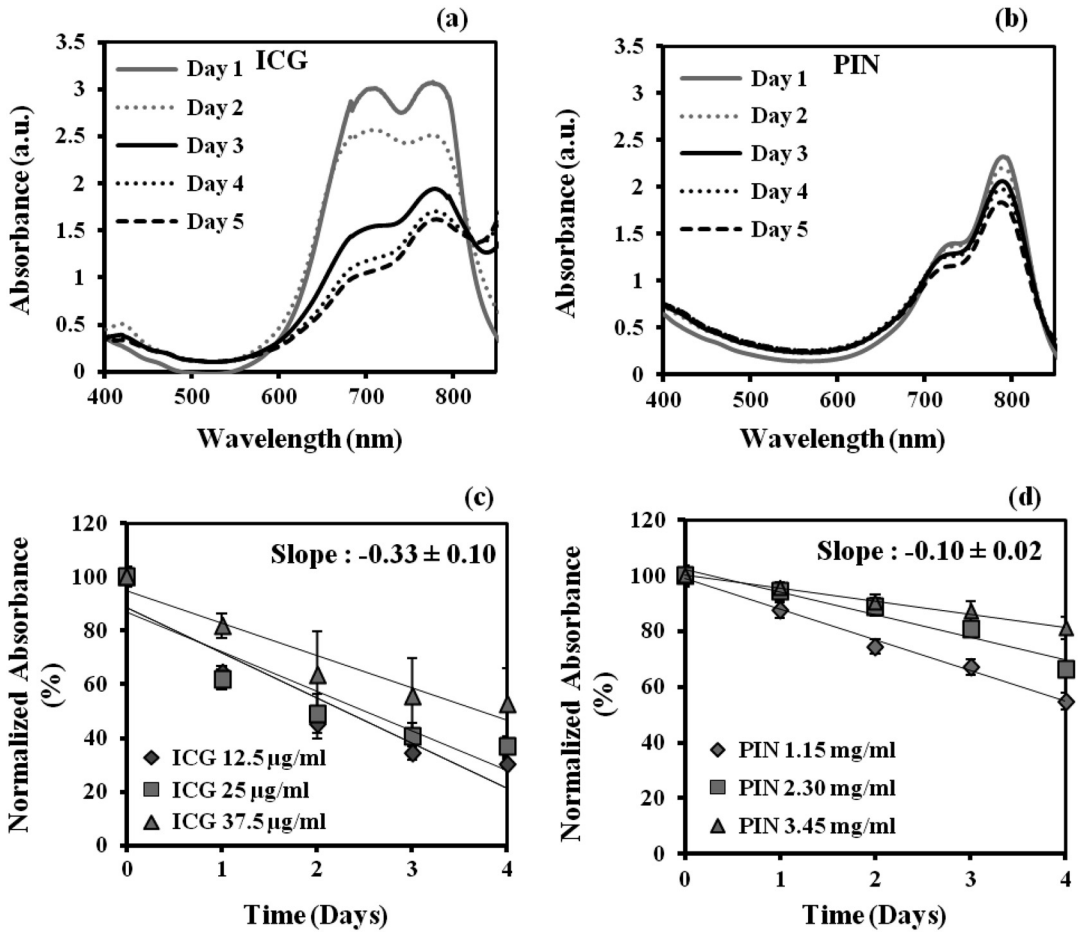

Fig. 5 Averaged absorption spectra of (a) ICG at 37.5 μg/ml and (b) PIN at 3.45 mg/ml taken at different days. Time-dependent changes in absorbance are shown for (c) ICG and (d) PIN at three concentrations ($n = 5$ for each concentration). The error bars are obtained by standard errors of mean. The labeled slopes are averaged across three concentrations with a unit of 1/day.

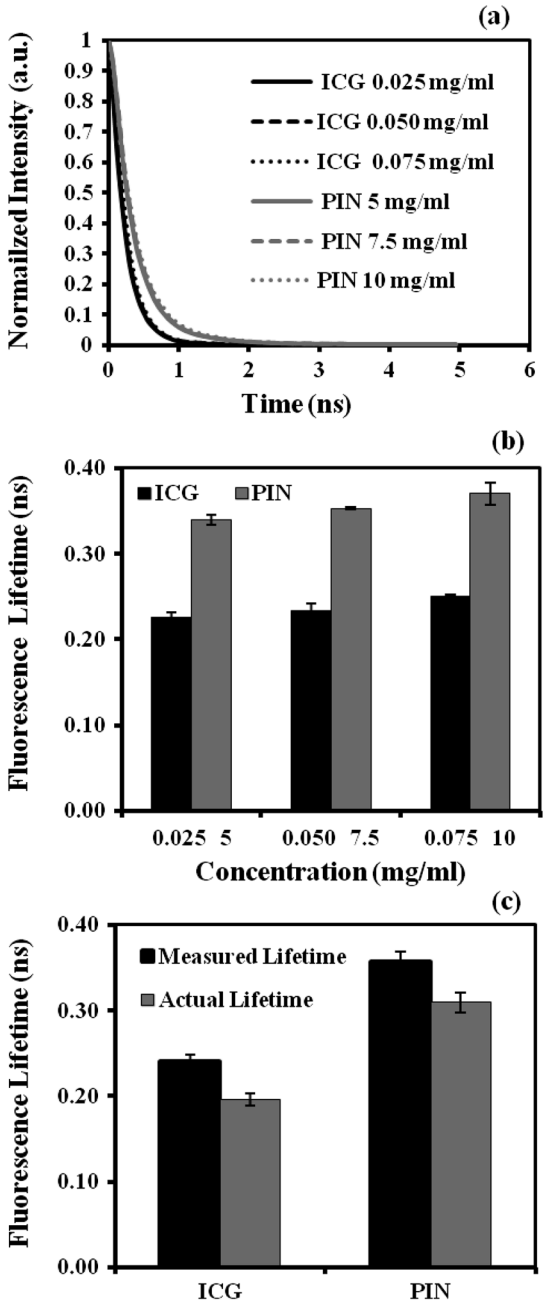

Fig. 6 (a) Normalized fluorescence decay curves for ICG and PIN at three different concentrations; (b) comparison of fluorescence lifetimes between ICG and PIN at three different concentrations; (c) comparison of the measured (without de-convolution) and actual lifetime (with de-convolution) values obtained for ICG and PIN ($n = 5$ for each case). The error bars are obtained by standard errors of mean.

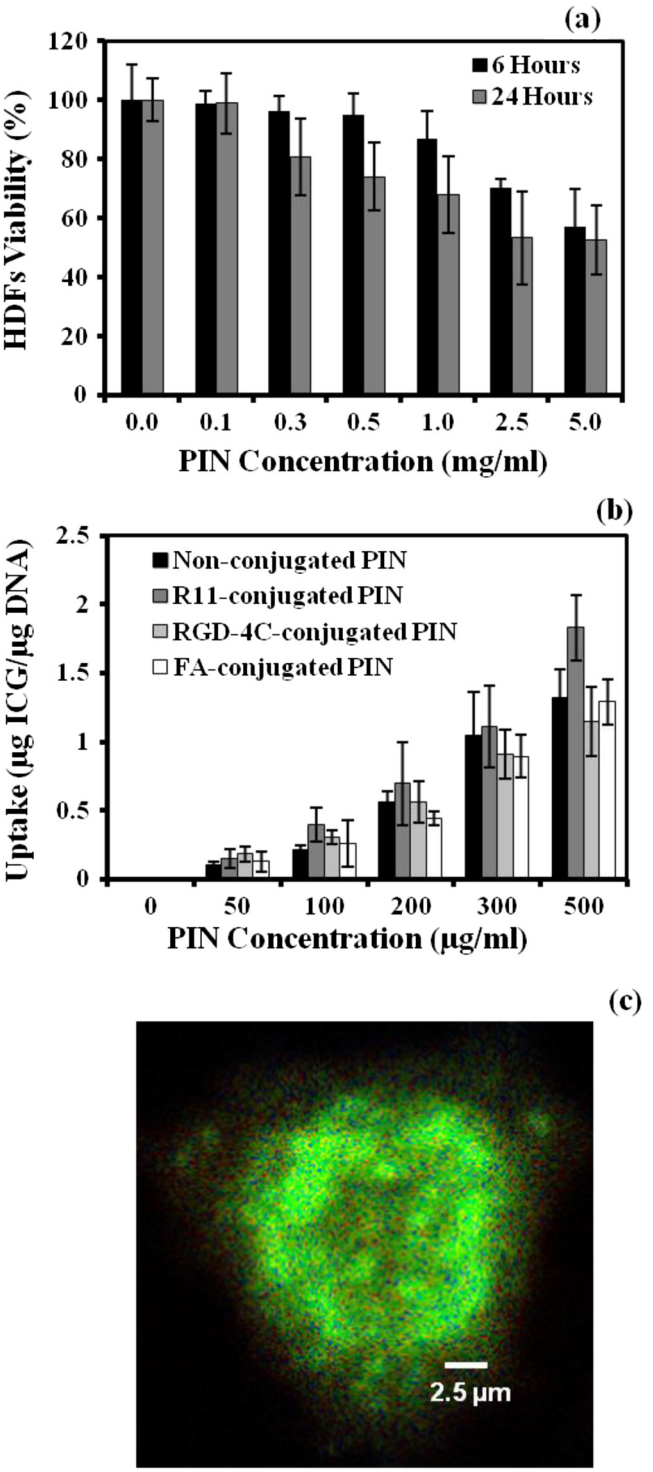

Fig. 7 (a) HDF cell viability study with seven different concentrations of PIN at six and 24 h ($n = 4$ for each concentration); (b) comparison of cellular uptake between nonconjugated PIN and PIN conjugated with R11, RGD-4C, and folic acid (FA) at five different concentrations of PIN ($n = 3$ for each group). The error bars are obtained by standard errors of mean; (c) A FLIM image of nonconjugated PIN uptaken by PC3 cells.

concentrations; it reveals that lifetime remains constant with the change in fluorophore concentration. Since lifetime, τ, is fluorophore concentration independent as seen from Fig. 6(a) and 6(b), we obtained an average τ of 0.24 ± 0.01 ns over three concentrations of ICG. In contrast, we observed that an averaged τ of PIN over three concentrations was 0.35 ± 0.01 ns, slightly longer than that of ICG. These results illustrate a lengthening effect of PLGA on the fluorescence lifetime of ICG, as shown in Fig. 6(b). However, our measured lifetime of ICG was a little longer than the lifetime value of ICG in published data.[20] Hence the influence of the system response on lifetime of ICG and PIN was studied. The response function obtained from white sample measurements gave a Gaussian curve with a narrow width of 80 ps. The obtained Gaussian curve was deconvoluted with the obtained ICG fluorescence decay curve. The resultant deconvoluted curve was further fitted

using Eq. (2) to obtain more accurate lifetime values. The similar method was applied to find the actual lifetime of PIN. Figure 6(c) represents the measured (without deconvolution) and actual (with deconvoltuion) lifetimes of ICG and PIN. It was observed that the lifetimes of ICG and PIN were decreased to 0.19 ± 0.01 and 0.30 ± 0.01 ns, respectively, after deconvolving the system-response function. Moreover, the obtained actual lifetime of ICG (0.19 ± 0.01 ns) became very close to the published lifetime value of 0.17 ns.[20,21] This part of observations reports (1) the lengthening effect of PLGA on the lifetime of ICG in PIN; (2) the consistency between our results and published lifetime of ICG; (3) the necessity to de-convolve the instrument response function for more accurate lifetime quantification.

3.3 *In Vitro Studies*

As shown in Fig. 7(a), the cell viability was obtained by MTS assay. After six hours, a significant cell viability of 85% was obtained with PIN concentrations up to 1 mg/ml. In case of the 24-h incubation, the cell viability was significant with PIN concentrations up to 0.5 mg/ml. However, cell viability reduced when higher concentrations of PIN (>1 mg/ml) were exposed to HDFs. PIN were cytocompatible with the healthy cells for lower concentrations and showed no toxic effects. Further, the results of the cellular uptake of ligand-conjugated PIN study indicated a significant uptake by R11-conjugated PIN as compared with nonconjugated, RGD-4C-conjugated, and folic acid-conjugated PIN, especially at 500 μg/ml, as shown in Fig. 7(b), presented by the fluorescence intensity. Hence R11 peptide exhibits the strongest ability of targetting prostate cancer as compared to RGD-4C and folic acid.

PC3 cells incubated with PIN were examined for their cellular uptake using FLIM. Figure 7(c) shows a FLIM image with strong fluorescence from a PIN-containing PC3 cell. The control PC3 cells without PIN, on the other hand, show no fluorescence. Overall, this figure confirms the presence of PIN that were indeed internalized within the cancer PC3 cells. In addition to that, a mean fluorescence lifetime of 0.58 ns was observed from these cells incubated with PIN. This mean lifetime value from FLIM is larger than the lifetime value of PIN (0.30 ns), obtained from the ICCD camera after deconvolution. Such a difference in lifetime between FLIM and our ICCD camera measurement could be attributed to two factors: (1) different instrumentation and also different solvents used for nanoparticle suspension;[21] (2) the lifetimes of PIN obtained from FLIM were determined without de-convolving the system response function from the measured data, which in principle may give a little longer lifetime than the actual one.

3.4 *Phantom Studies*

The ability of PIN as an imaging contrast agent for DOT was investigated through a phantom experiment. Figure 8(a) represents the changes in optical density (ΔOD) obtained from multiple source-detector channels (represented by different colors), when the absorbing sphere (0.9 cm in diameter and containing PIN of 2.08 mg/ml) was moved from 3- to 2-cm and then to 1-cm depth below the probe array surface. The *y* axis shows ΔOD changes with an arbitrary unit, whereas the *x* axis represents the time (in sec) during which data was captured, and the sphere was moved from deeper to shallower depths. As observed from the plot, at 3-cm depth, a very small increase in ΔOD was obtained from time periods of 30 to 60 s and 90 to 120 s, while

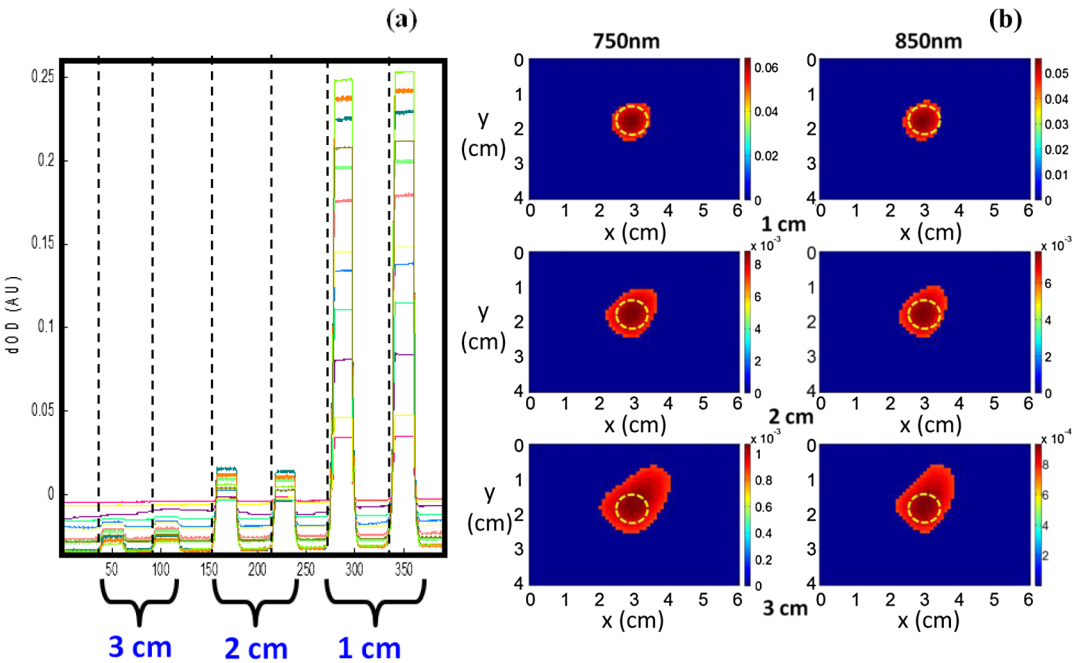

Fig. 8 (a) Plot of ΔOD measurements with time scale (in sec) from a liquid-tissue phantom with an embeded PIN-containing sphere, placed at 1-, 2-, and 3-cm depth below the phantom top surface [see Fig. 2(b) and 2(c)] different lines represent the data taken from different source-detector channels; (b) reconstructed 2D DOT images of ΔOD due to the PIN-containing sphere embedded in the phantom at 1-, 2-, and 3-cm depths (from top row to bottom row, respectively). The left column represents the ΔOD images obtained at 750 nm at the three depths, while the right column exhibits the ΔOD images obtained at 850 nm at the respective depths, too. The images are obtained with a threshold of 80% of maximum. The color bar represents ΔOD changes measured at the surface. The unit for *x*- and *y*-axis is cm. The dashed curcles represent the actual size and location of the embeded sphere.

significant increases in ΔOD were achieved at 2-cm and 1-cm depth for all of the channels. In principle, as the sphere moves nearer to the surface, more light is absorbed by the embedded sphere containing PIN, and less light is detected by the detector. This is the reason why we observed more increases in ΔOD when the PIN-containing sphere was at shallower depths. However, when being placed at 3-cm depth, the embedded sphere still provided us with a significant contrast for distinct ΔOD images.

Figure 8(b) represents 2-D reconstructed DOT images of ΔOD at 750 and 850 nm for the embedded sphere. The reconstructed DOT images are obtained as 2-D forms by setting or forcing the reconstructed images at appropriate depths of 1, 2, and 3 cm, respectively.[17] The color bars represent the recovered changes in OD based on the optical measurements at the phantom surface. The final reconstructed images are obtained at a cutoff threshold of 80% of the maximum. Note that the reconstructed ΔOD values are much larger (1 to 2 orders of magnitude) when the embedded PIN-containing sphere is at a shallower depth than those at deeper depths. Namely, larger reconstructed ΔOD intensities and thus more contrasts are observed when the spheres are placed at 1-cm and 2-cm depths, respectively, as compared with those with the sphere at 3-cm depth. But a significant contrast is still clearly shown at the 3-cm depth in this figure, while the reconstructed images become less focused with a lower spatial resolution for a deeper-located sphere. This is expected because a deeper object involves more diffuse light and returns more scattered optical signals. Similar results were also observed when repeated measurements were performed with different PIN concentrations (data not shown). Overall, these results confirm that PIN can hold light absorption feature and serve as a contrast enhancer for DOT.

The heating ability of ICG and PIN was analyzed through a thermal ablation study. Figure 9(a) and 9(b) show the peak temperature changes achieved after irradiating the phantom with the laser for 5 min, from each of the phantoms at 3-, 5-, and 7-mm lateral distance as well as in depth. A gradual decrease in temperature is observed with an increase in lateral distance and in depth from 3 to 7 mm for all phantoms. This signifies a spatial distribution of heat achieved in the area near by the laser tip and also in the area right below the laser tip, as compared with the surrounding area of the phantom. Specifically, Fig. 9(a) illustrates that the temperature increase in the control phantom (~4 °C) was 2 to 2.5 times smaller than that in ICG and PIN phantoms (~8 to 10°C), at 3 mm away from the laser tip. This implies that PIN possess the great absorbing and heating ability similar to that of ICG, leading to augmented thermal effects and possible tissue hyperthermia for future cancer treatments.

Moreover, it was observed from Fig. 9(a) and 9(b) that the concentrations of free ICG used were about 110 to 260 folds less than the ICG concentrations in PIN for the three different concentration cases, while the respective heating effects achieved similar increases in temperature in both ICG and PIN phantoms. In order to achieve such similar thermal effects in both kinds of phantoms, we first measured the absorbance of PIN at a concentration of 2.08 mg/ml in water and then tried to optimally match the absorbance with different concentrations of free ICG dissolved in water. It was observed that the concentration of 0.008 mg/ml for free ICG showed the best matching absorbance ($A = 2.5$) as compared with that from PIN at 2.08 mg/ml ($A = 2.6$). According to the loading

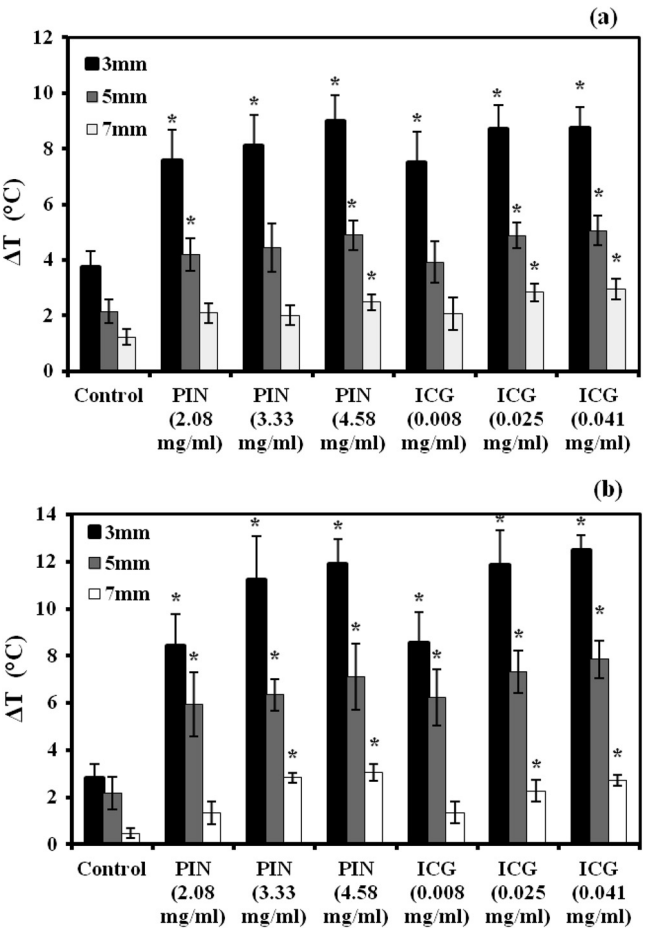

Fig. 9 Peak changes in temperature at 3, 5, and 7 mm (a) in lateral distances and (b) in depths for Control, PIN, and ICG phantoms ($n = 4$ for each case). The error bars are obtained by standard errors of mean. "$*$" means statistically significant difference ($p < 0.05$) with respect to the temperature obtained from the control phantom.

efficiency of PIN, it was also found that 2.08 mg/ml of PIN contained 0.01 mg/ml of free ICG, very close to the amount of ICG (0.008 mg/ml) used in the ICG phantoms. This is why we achieved similar temperature rises in both ICG and PIN phantoms, in three different levels of concentrations, while the respective concentrations of ICG in these two types of phantoms were about 110 to 260 folds different between them.

Last, Fig. 9(b) illustrates that for depth-dependent measurements, the temperature increases in the control (~3 °C) were about two to three times smaller than the other two cases (~8 to 9°C). Hence the depth measurements have shown a considerable heat spread until 5 mm below the laser tip in both the ICG and PIN phantoms with respect to the control phantoms. In addition, it was observed that the peak temperatures achieved in depth-dependent measurements were higher than those in distance-dependent measurements. This is perhaps because the phantoms were a little melted at the top due to 5-min irradiation of laser, which shortened the distance from the phantom top surface to the thermocouple wire poked at various depths (Fig. 4). Depth-dependent measurements hence gained higher temperatures under thermal effects of laser irradiation. Overall, the temperature measurements at different lateral distances (to ~5 mm) and depths (~5 mm) validate the capability of PIN to serve as

a thermal ablation agent and lead to two to three times more thermal impacts on the irradiated regions, possibly sufficient to create photo-thermal effects to destroy tumors.

4 Conclusion and Future Work

Multifunctional PIN were succesfully synthesized with a mean particle size of 246 nm and 48.5% of ICG entrappment efficiency. The optical characterization of PIN in terms of excitation-emission spectra, flourescence intensity, and absorption spectra demonstrated the stability of PIN as compared with free ICG in various biorelevant solvents over an extended period of time. It was also observed that PIN play an important role in preserving the optical porperties of ICG. The fluorescence lifetime of free ICG obtained was 0.19 ns, whereas it for PIN was increased to 0.30 ns due to the encapsulation of ICG within PLGA shell. The cell viability study verified the cytocompatibility of PIN, while the cellular uptake study confirmed the high binding efficiency of R11-conjugated PIN with PC3 cells. Furthermore, PIN were successfully able to result in significant temperature gains (two to three times) that may be required for hyperthermia treatments of cancer, using gelatin-intralipid phantoms studies. The overall results in this study suggest that PIN (1) have the great potential to induce local hyperthermia in tissue within 5 mm both in radius and in depth; (2) result in improved optical stability, excellent biocompatibility with healthy cells at lower concentrations without much toxic effects, and a great targeting capability; (3) have the ability to serve as an image contrast agent for deep tissue imaging in DOT.

Since this study has been based on laboratory tissue phantoms and *in vitro* cell culture experiments, further investigation using animal models may be needed to examine the feasibility of PIN to be useful for *in vivo* clinical research and cancer treatment. Specifically, several important parameters, such as concentrations of PIN, irradiation period and power of the laser, and the desired particle size of PIN are critical and need to be determined for any possible translation research. In particular, the particle size of PIN determines the delivery efficiency for cancer targeting since large PIN sizes may prevent them from going through small vessels to arrive at the targetted sites. Also, the application of PIN as a DOT contrast agent can be studied with the animal model, too. Overall, multifunctional PIN can be thus applied for various optical imaging modalities, such as to be used to enhance photoacoustic imaging.

Acknowledgments

This work was supported in part by the DOD prostate cancer research program (W81XWH-09-1-0406). The authors acknowledge Professor I. Gryczynski from the University of North Texas Health Science Center for his generous help with FLIM measurements.

References

1. S. Gioux, H. Choi, and J. V. Frangioni, "Image-guided surgery using invisible near-infrared light: fundamentals of clinical translation," *Mol. Imag.* **9**(5), 237–255 (2010).
2. E. I. Altinoglu et al., "Near-infrared emitting fluorophore-doped calcium phosphate nanoparticles for in vivo imaging of human breast cancer," *ACS Nano.* **2**(10), 2075–2084 (2008).
3. X. Zheng et al. "Indocyanine green-containing nanostructure as near infrared dual-functional targeting probes for optical imaging and photothermal therapy," *Mol. Pharm.* **8**(2), 447–456 (2011).
4. T. H. Kim et al., "Evaluation of temperature-sensitive, indocyanine green-encapsulating micelles for noninvasive near-infrared tumor imaging," *Pharm. Res.* **27**(9), 1900–1913 (2010).
5. V. Saxena, M. Sadoqi, and J. Shao, "Enhanced photo-stability, thermal-stability, and aqueous-stability of indocyanine green in polymeric nanoparticulate systems," *J. Photochem. Photobiol. B: Biol.* **74**(1), 29–38 (2004).
6. V. Ntziachristos et al., "Concurrent MRI and diffuse optical tomography of breast after indocyanine green enhancement," *Proc. Natl. Acad. Sci. USA* **97**(6), 2767–2772 (2000).
7. R. X. Xu et al., "Fabrication of indocyanine green encapsulated biodegradable microbubbles for structural and functional imaging of cancer," *J. Biomed. Opt.* **14**(3), 034020 (2009).
8. Y. Tang and A. J. McGoron, "Combined effects of laser-ICG photothermotherapy and doxorubicin chemotherapy on ovarian cancer cells," *J. Photochem. Photobiol. B: Biol.* **97**(3), 138–144 (2009).
9. A. J. Gomes et al., "Indocyanine green nanoparticles useful for photomedicine," *Photomed. Laser Surg.* **24**(4), 514–521 (2006).
10. Y. Tang et al., "Simultaneous delivery of chemotherapeutic and thermal optical agents to cancer cells by a polymeric (PLGA) nanocarrier: an *in vitro* study," *Pharm. Res.* **27**(10), 2242–2253 (2010).
11. Y. Kohl et al., "Preparation and biological evaluation of multifunctional PLGA-nanoparticles designed for photoacoustic imaging." *Nanomed.: Nanotech. Biol. Med.* **7**(2), 228–237 (2011).
12. J. D. Byrne, T. Betancourt, and L. Brannon-Peppas, "Active targeting schemes for nanoparticle systems in cancer therapeutics," *Adv. Drug Deliv. Rev.* **60**(15), 1615–1626 (2008).
13. J. Zhou et al., "Analysis of oligo-arginine cell-permeable peptides uptake by prostate cells," *Amino Acids* **42**(4), 1253–1260 (2012).
14. O. C. Farokhzad et al., "Nanoparticle-aptamer bioconjugates: a new approach for targeting prostate cancer cells," *Cancer Res.* **64**, 7668–7672 (2004).
15. S. Dhara et al., "Targeted delivery of cisplatin to prostate cancer cells by aptamer functionalized Pt (IV) prodrug-PLGA-PEG nanoparticles," *Proc. Natl. Acad. Sci. USA* **105**(45), 17356–17361 (2008).
16. Z. J. Lin et al., "Time-gated optical imaging detect positive prostate cancer margins," *Proc. SPIE* **7161**, 716119 (2009).
17. T. J. Huppert et al., "HomER: a review of time-series analysis methods for near-infrared spectroscopy of the brain," *Appl. Opt.* **48**(10), D280–D298 (2009).
18. M. A. Yaseen et al., "Laser-induced heating of dextran-coated mesocapsules containing indocyanine green," *Biotech. Prog.* **23**(6), 1431–1440 (2007).
19. V. Saxena, M. Sadoqi, and J. Shao, "Indocyanine green-loaded biodegradable nanoparticles: preparation, physicochemical characterization and in vitro release," *Int. J. Pharm.* **278**(2), 293–301 (2004).
20. A. Gerega et al., "Wavelength-resolved measurements of fluorescence lifetime of indocyanine green," *J. Biomed. Opt.* **16**(6), 067010 (2011).
21. M. Y. Berezin et al., "Engineering NIR dyes for fluorescent lifetime contrast," *31st Annual International Conf. of the IEEE EMBS, Con. Proc. IEEE Eng. Med. Biol. Soc.* 114–117 (2009).